

# DEVELOPMENT OF THE NUMERICAL MODEL OF THE NEW-BORN CHILD DUMMY Q0

**Christian Gehre**

**Volker Schindler**

Technical University of Berlin

Germany

Paper Number 05-0074

## ABSTRACT

The European research project "CHILD" (Child Injury Led Design) is working on the improvement of passive safety of children as occupants in cars. One of the objectives is to develop new child dummy models. This paper focuses on the development of the finite element model of the new-born child dummy Q0 for the use with LS-Dyna.

The Q0 model was created by using the CAD models of the hardware-Q0. All non-rigid body segments such as head, neck and torso were validated by using results of component tests. Optimisation tools were used to identify the adequate material models for the body segments and to define the parameters of these materials.

The response of the dummy database in these calibration test procedures correlates well with the physical Q0 dummy. Furthermore, all parts would pass the certification requirements.

## INTRODUCTION

The new-born child dummy Q0 (Figure 1), developed by TNO and FTSS was one of the first results of the CHILD project. The numerical model is based on this first series of Q0 dummies.

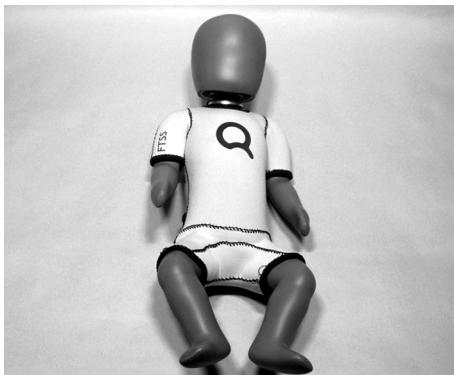


**Figure 1. Child dummy Q0.**

The Q0 represents a six week old infant with a mass of 3,400 grams and a sitting height of 355 mm. It

was designed for the use with child restraint systems (CRS) for this age group in frontal, lateral, rear and roll-over crash configurations. Compared to the P0 and the CAMI dummy, it offers the opportunity to measure head, chest and pelvis accelerations as well as the upper neck forces and torques. So it is now possible to assess the protection level of child restraints of this age group by using physical measurements on the dummy.

## METHOD

The dummy model was designed and validated for the use with the finite element solver LS-Dyna 970, release 3858.

Those parts of the dummy, which are designed to be non-deformable in a crash test, are made as rigid bodies in the model to reduce the total computing time. All other parts of the model, such as skin of the head, rubber of the neck or torso foam are using non-rigid materials to describe the material behaviour of these dummy parts.

All non-rigid parts were validated by using results of component tests with these parts or an assembly with these parts involved. Furthermore results of a thorax impact test of the complete dummy were used to validate the model.

The choice of the material models of every dummy part was proven by comparison with the corresponding parts of other existing numerical dummy models, designed for the use with LS-Dyna. However, no material model or its material parameters of other dummies were transferred directly to the Q0 dummy model.

## STRUCTURE OF THE DUMMY MODEL

Figure 2 shows the Q0 dummy model. It has a skull, a neck, a rigid thoracic spine, a lumbar spine, which is identical to the neck and a rigid pelvis. The torso part made of foam covers the internal structure of the dummy from the pelvis up to the shoulders. The bent arms and legs are directly screwed to the upper thoracic spine and the pelvis, respectively. Their only

degree of freedom is the rotation around the transverse axis.

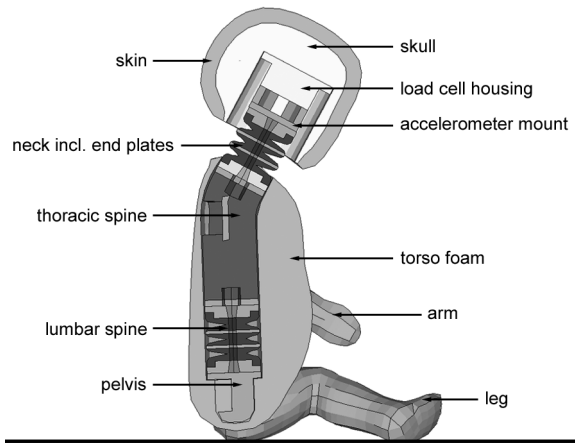


**Figure 2. Structure of the Q0 dummy model.**

The FEA mesh of all parts is made of solid elements, mainly of six-node hexagon and five-node pentagon elements. The surface of some parts is covered with a thin layer of shell elements. It is used as interface for contacts to other parts of the dummy and the surrounding areas. In total 7,500 nodes, 2,000 rigid elements and 11,000 deformable elements were used for the dummy besides the suit.

The total computing time of the dummy without any environment, such as CRS, is approximately 13 seconds for every millisecond of simulation time on a Pentium 4 3.0 GHz machine.

### Head

The head assembly is made of skull including skin layer, upper neck load cell and accelerometer mount. A visco-elastic material model was used for the skin and an elastic model for the beam of the load cell. This beam connects the skull with the load cell housing. Skull, load cell housing and accelerometer mount are made of rigid material.

A version with a non-rigid skull was also simulated, but the non-rigid material had no advantage over the rigid version. The computing time was longer and the numerical stability was less than for the rigid version.

The head is equipped with two sensors, a six-axial load cell to measure forces and torques in the upper neck of the dummy and a tri-axial accelerometer.

### Neck and lumbar spine

The structure of the neck (Figure 3) is similar to the neck of Hybrid III dummies. The main part, the neck

mould, is made of rubber and includes two metal end plates and two metal intermediate disks. A non-pre-tensioned steel cable, fixed between the two end plates, restricts the neck tension. Three slits at the front side of the neck mould are reducing the stiffness in rearward bending conditions.

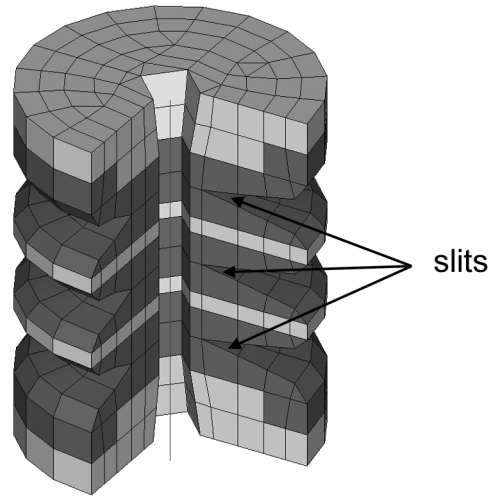


**Figure 3. Model of the neck.**

The comparatively small and soft neck is very sensitive against the density of the used mesh. Some important geometrical details, such as the geometry of the slits, are lost by using a wider FEA mesh. The used fine mesh is a compromise of computing time, numerical stability and response of the upper neck load cell in the validation tests.

A second model of the neck with an increased computing time efficiency was validated in parallel.

The lumbar spine joint is identical to the neck assembly. It is mounted in upside down position with slits to the back of the dummy.

### Thoracic spine and pelvis

The thoracic spine is made of rigid material. A tri-axial accelerometer measures the chest acceleration. The arms are connected to the spine top plate.

The pelvis of the dummy is made of steel. So rigid material has been used in the model. Furthermore the pelvis is equipped with a tri-axial accelerometer.

### Torso and rubber suit

The torso flesh foam covers the skeleton of the dummy from the shoulders to the pelvis. It has a cut on the rear side from the upper pelvis to the lower neck to allow the assembly of the dummy. The cut is closed by the suit of the dummy.

Solid elements are also used for the torso part, but compared to the others, the solid mesh consists only of tetrahedron elements.

The Q0 dummy is provided with a suit, which covers torso, upper arms and upper legs. Until now it is not included in the numerical model. It will be provided with a later version of the model. The suit is not only necessary because of the additional soft layer on the dummy's surface, it also covers the gaps between extremities and torso.

The torso foam is fixed to the dummy's skeleton only by using contacts. No node or element is attached to another part of the dummy.

### Extremities

Arms and legs are made of the same PVC-based material. They are attached with bolts to the top spine plate and the pelvis, respectively.

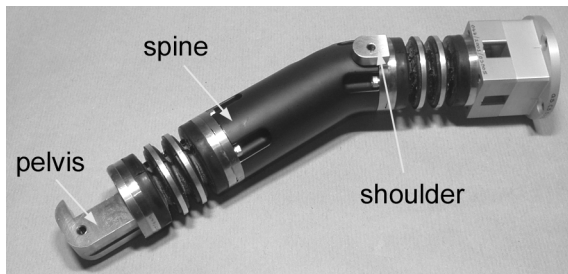


**Figure 4. Skeleton of the Q0.**

Figure 4 shows the skeleton of the Q0 including the top plate of the thoracic spine with the simplified rigid shoulder and the pelvis. Arms and legs are made of the same material.

## VALIDATION PROCEDURES

Head and neck have to pass several certification tests [4] to show the biofidelity and to get the approval for the use in crash tests. Results of these tests were used to validate the model. Furthermore, some additional component tests with neck, torso and extremities, and thorax impact tests with the complete dummy were performed to obtain more data for the validation.

The software tool Altair Hyperstudy was used to vary the material parameters and to get an optimised model.

### Head

The head assembly was validated by using three different set-ups of head drop tests (Table 1). Both tests with drop height of 130 mm are part of the certification procedures. The third one, a 45° frontal impact

test with a drop height of 376 mm, is taken from the certification procedures of CRABI 12 month old child dummy [1].

**Table 1. Set-up of head validation tests.**

Impact direction	Drop height	Angle
frontal	130 mm	28°
lateral	130 mm	35°
frontal	376 mm	45°

Not only the maximum head acceleration was used to validate the model of the head assembly. Also the shape of the acceleration curve should correlate with the experiment. The width of the signal is also described by the  $a_{3ms}$  value. So it was used as secondary parameter for the validation.

The maximum resultant head acceleration has to be between 91 g and 157 g in frontal and 94 g and 162 g in lateral direction to pass the certification requirements [4].

### Neck

Two different test set-ups were used to validate the head-neck assembly in flexion, extension and lateral bending. In all lateral bending tests the head was mounted on the neck rotated by 90° around the vertical axis (rearward position) in order to have symmetrical neck loading.

In the first configuration the neck was mounted on a sled, which was accelerated by a pneumatic catapult. Figure 5 shows the set-up of the flexion bending test. In all tests there was no contact between chin and mounting device.

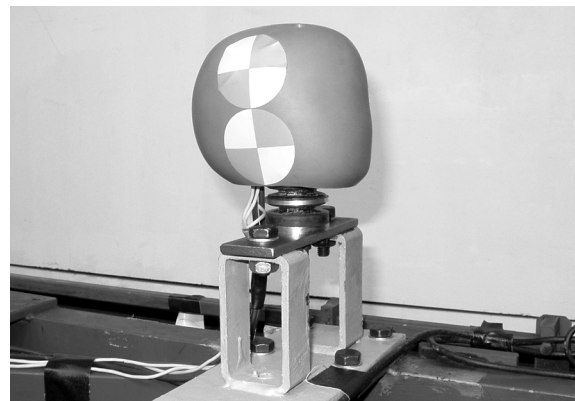


**Figure 5. Set-up of sled test.**

The second configuration, a pendulum test, is part of the certification procedures. The pendulum is described in Part 572 subpart E [2].

Figure 6 shows the average crash pulses of the pendulum and the sled tests. The average impact velocity was about 3.37 m/s in the pendulum tests and 4.12 m/s in the sled tests.

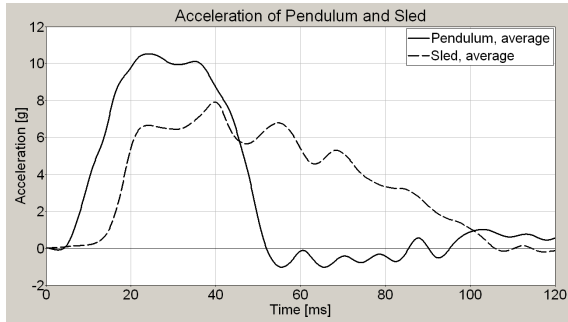


**Figure 6. Acceleration in sled and pendulum tests.**

The head rotation angle, the upper neck forces and torques were used as main target values to validate the model. Additionally the neck moment at the occipital condyles (OC-joint), a combination of neck moment and shear force, was used. The calculation of these moments is shown in (1), (2) and (3).

$$M_{xOC} = M_x + 0.033 \text{ m} \cdot F_y \quad (1)$$

$$M_{yOC} = M_y - 0.033 \text{ m} \cdot F_x \quad (2)$$

$$M_{zOC} = M_z \quad (3)$$

The moment at the OC-joint was used as simplified indicator of a correct time dependent course of neck forces and moments.

### Torso foam

The torso part was validated by using results of two different test set-ups. Firstly, a simple drop test with the torso foam was used to pre-validate the model and secondly, a thorax impactor test with the complete dummy for the final validation (Figure 7).

The computing time of a single thorax impact test by using the complete dummy is comparably long. So the drop test was used to make a quick pre-selection of the material model and the range of variation of material parameters. Thus it was possible to reduce the total time of validation of the torso foam. The final validation of the foam was done with the complete dummy including all functions such as internal contacts and

the fixation of the extremities to the skeleton with joints.

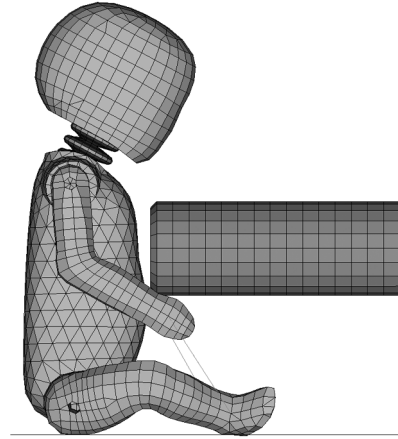


**Figure 7. Set-up of thorax impactor test.**

The arms of the dummy in the thorax impactor test were fixed at the legs with tape material. The mass of the impactor was about 2.6 kg and the impact velocity was 2.2, 3.2 and 4.3 m/s. The torso drop test were performed with the same velocities.

Based on the longitudinal accelerations of chest and impactor the maximum chest deflection and impact force were calculated. Both parameters were used for the validation of the torso foam.

### Extremities

The extremities are not included in the certification procedures of the Q0. Therefore simple drop tests with different impact velocities, taken from the torso tests, were performed to get data to validate arms and legs of the model. Arm and leg were fixed with tape with their inner side under a steel plate (Figure 8). So load was applied to the parts in lateral direction.



**Figure 8. Set-up of arm drop test.**

Following the validation of the head, peak and  $a_{3ms}$  value of the vertical impactor acceleration were used as main parameters of the validation.

## RESULTS

The sign conventions of the SAE J211 standard are used in the experiments and simulations for all measured values. Also all plots of these measures follow this standard.

### Head

The head assembly was validated by varying the material model and the material properties of the skin layer of the head. All used material models have a visco-elastic characteristic. Finally MAT\_062, a non-linear viscous foam, originally made for the rib padding of the EuroSID [3], was selected for the skin. The response of a linear material model cannot be as exact as a non-linear model at different impact velocities in this application.

The ratio between head acceleration in the frontal and in the lateral impact test with a drop height of 130 mm was the main problem in the validation. It has to be approximately 1.05, but finally 0.94 was achieved with MAT\_062, the best compromise of all tested materials.

**Table 2. Maximum head acceleration.**

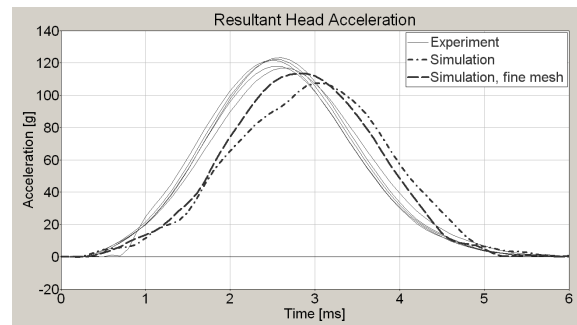
Set-up	Experiment	Simulation
frontal, 28°, 130 mm	116.6 g - 122.8 g av. 120.0 g	107.3 g
frontal, 45°, 376 mm	237.0 g - 276.3 g av. 254.9 g	273.9 g
lateral, 35°, 130 mm	110.6 g - 116.7 g av. 114.1 g	113.7 g

However, the maximum head acceleration as well as the  $a_{3ms}$  value correlate well with the experiment. Table 2 shows the maximum head acceleration of the finally selected and optimised viscous foam MAT\_062. So the model fulfils the requirements of the certification tests.

The main influence parameters on the maximum head acceleration are the initial Young's modulus ( $E_1$ ) and the exponent in power law for Young's modulus ( $n_1$ ) [3]. A declining  $E_1$  or  $n_1$  reduces the maximum head acceleration and the width of the acceleration curve. In this case the  $a_{3ms}$  value increases. The influence of  $E_1$  and  $n_1$  increases with the impact velocity.

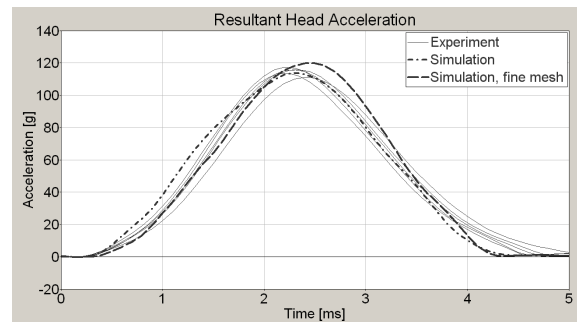
Except for the Poisson's ratio, which has only a slight influence on the head response, all other parameters of MAT\_062 have in principle the same behaviour as  $E_1$  and  $n_1$ .

Figure 9 shows the acceleration curves of experiments and simulation in the 28° frontal impact configuration. The gradient of the acceleration in the model is lower than in the test. Additional simulations using MAT\_062 and a mesh of smaller elements improved the shape of the curve, especially between 1.5 and 3.0 ms. At the same time the gradient of the declining edge gets slightly too high. A fine mesh generally stiffens the material, and the maximum acceleration increases.



**Figure 9. Head response in the 28° frontal impact.**

The effect of stiffening the material to improve the shape of the curve affects also the other tested configurations. The shape of the head acceleration curve in the 45° frontal impact and the 35° lateral impact (Figure 10) correlates better with results of the experiments than in the 28° frontal impact.



**Figure 10. Head response in the 35° lateral impact.**

However, the achieved results already show a good agreement with target values of the experiments. Modifications of the skin's mesh could improve the shape of the acceleration curves. Therefore in a next step the mesh of the skin will be modified and the material parameters will be adapted to this new mesh.

## Neck

The model was validated by varying the type of visco-elastic material, the material properties, the thickness of the contact between the neck segments and level of detail of the FEA-mesh. MAT\_006, a simple linear visco-elastic material model, was finally selected for the rubber parts of the neck. Other, more detailed visco-elastic materials of LS-Dyna offer more parameters to adapt the material in detail, but they had no advantage in this application. Furthermore the computing time of the neck was rather high when using these materials.

There are four parameters available in MAT\_006, the elastic bulk modulus (BULK), a short-time (G0) and a long time (GI) shear modulus and finally the decay constant (BETA). Not all of them have the same effect on upper neck shear force, bending moment and head rotation angle.

The angle in all three loading configurations is mainly affected by the long-time shear modulus. An increasing GI reduces the head angle. The shear force is mainly influenced by G0 and BETA. They have opposite influence. An increasing G0 or a decreasing BETA are increasing the absolute shear force. The bending moment is mainly influenced by G0 and GI in extension bending and by BULK in flexion and lateral bending. Increasing BULK and G0 reduce and an increasing GI rises the measured torque.

A thick contact area reduces the bending angle of the neck, but it also has an influence on the moments. The torque is increasing under flexion bending and decreasing under extension bending with a thicker contact area.

MAT\_001, an elastic material was chosen for the steel cable of the neck. The only varied influence parameter was Young's modulus E. Modifications of the cable stiffness affects mainly the rotation angle of the head, especially in the pendulum tests. A stiffer cable material reduces the angle.

The Young's modulus of the cable was only varied in the neck pendulum test set-up.

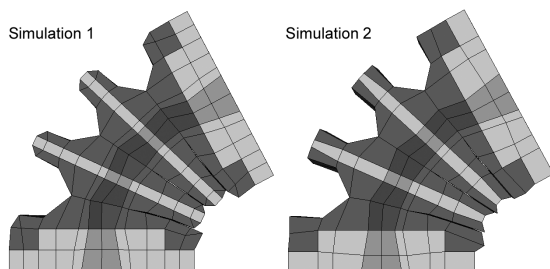


**Figure 11. Different models of the neck in flexion test at 90 ms.**

The structure of the FEA mesh of the neck is an important parameter for the overall performance of the neck model. Figure 11 shows the two different detailed neck models used. The fine mesh (Simulation 1) was firstly created and validated. Based on these experiences a less detailed mesh (Simulation 2) was created with the focus on computing time. So it was possible to reduce the computing time by 25% while keeping the same response characteristic.

### Neck sled tests

First of all the neck was validated by using the results of the sled tests. Afterwards the material properties were slightly adapted to also fit to the pendulum tests. All diagrams with results of the sled tests show the response of the neck with material, validated only for this configuration. The results differ slightly, when the final material, resulting from the sled and pendulum tests is used.

The model of the neck was validated by using the same priority of flexion, extension and lateral bending. So the validated model is a well balanced compromise.

Figure 12 shows the neck moment at the OC-joint versus the head rotation angle in the flexion bending test. The neck is slightly too stiff, but there already is a good correlation of simulation and experiment.

The peak at an angle of 7° in the rebound phase of the neck is coming from the shear force signal and is probably caused by contact problems of the neck and the stiff neck cable. This phenomenon also occurred in simulations with a higher pulse, but disappears when using a softer cable. However, in none of the simulations any element of the neck collapsed.

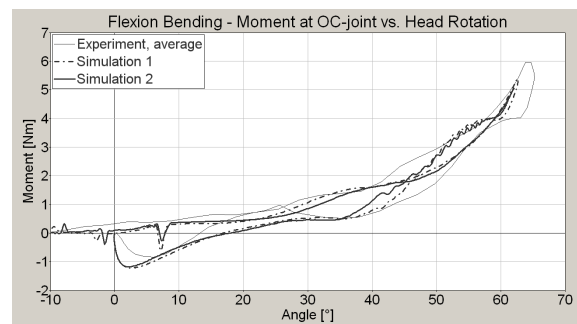


**Figure 12. Neck flexion performance in sled test.**

The response of the neck in the flexion bending test is shown in detail in Figure 13. While shear force  $F_x$ , head rotation angle are well correlated to the experiment, the moment  $M_y$ , the base of the OC-moment, is approximately 50% less than required. A change of the position of the sensor element within the load cell or a change of the centre of gravity of the head could

change this problem easily, because of the different length of the internal lever arm. However, both information are directly taken from the dummy and should not be modified. Furthermore, the extension and the lateral bending tests point out the correct position of both factors. So the only remaining option, is the modification of the material properties to increase  $M_y$ . All trials to increase the moment had too negative effects on the results of the extension and lateral bending response of the neck. The relevant deviation of  $M_y$  between experiment and simulation starts at 70 ms. At this time the head rotation angle reaches 50°. The contact between chin and chest limits the head rotation in the assembled dummy to this angle. So the problem of the missing moment is less critical and the deviation can be accepted.

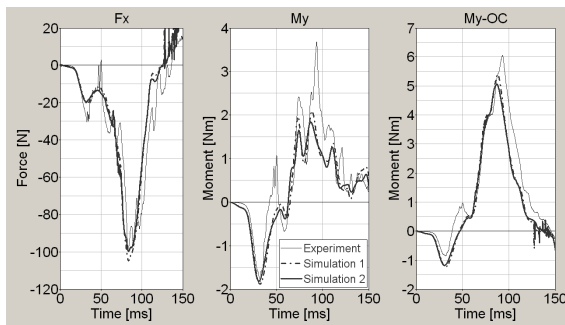


Figure 13. Neck response in flexion bending test.

The response of the neck in extension bending (Figure 14) and lateral bending (Figure 15) correlates well to the experiments up to a head angle of approximately 40°. The moment at the OC-joint is slightly too high in both load cases. The deviations of the single signals from the experiments are clearly smaller than in the flexion bending test.

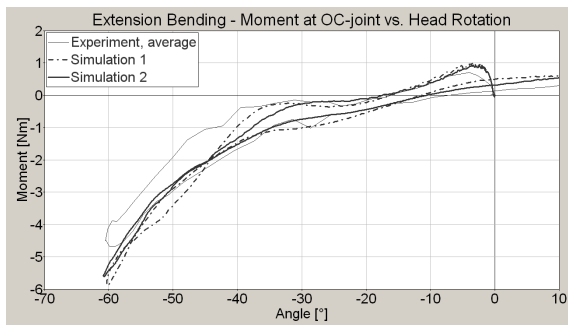


Figure 14. Neck extension performance in sled test.

The achieved correlation of the response of both neck models in all tested configurations is a good base

for the second step, the validation by using the neck pendulum test set-up.

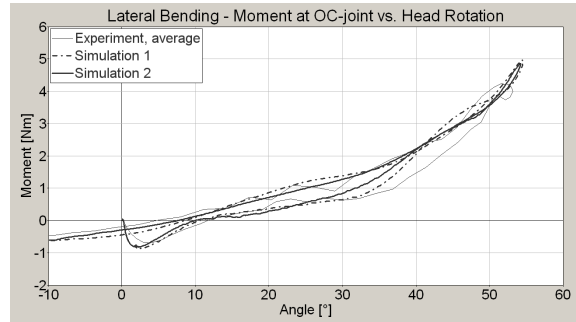


Figure 15. Neck lateral flexion performance in sled test.

**Pendulum tests**

The response of the neck models, validated only by using the sled tests, is already close to the results of the neck pendulum tests. Solely the head rotation differs significantly from the requirements. The validation started by varying the stiffness of the neck cable. These modifications have only limited influence on the upper neck shear force and bending moment. So the global response of the neck is not changed.

Figure 16 shows the response of the neck in the flexion test set-up. The results of both neck models are very close to the experimental data and within the biomechanical corridor of the neck flexion of a newborn child [4]. Furthermore the certification corridor at 50° is met by the numerical model.

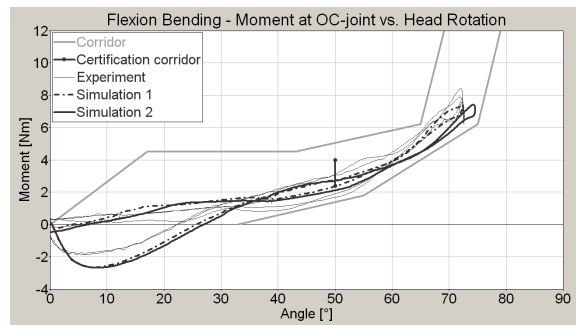
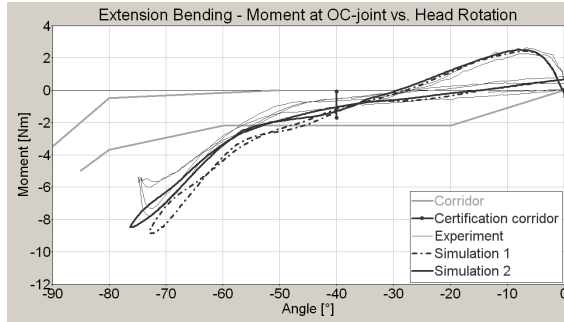


Figure 16. Neck flexion performance in pendulum test.

The model of the neck complies with the experimental data under extension loading up to 40° (Figure 17). Above this bending angle the model as well as the dummy leaves the biomechanical corridor. However, both models of the neck meet the certification requirements. The less detailed model

(Simulation 2) correlates slightly better to the experimental data than the more detailed one.



**Figure 17. Neck extension performance in pendulum test.**

The quality of the neck’s response in lateral bending is similar to the extension test. Above an angle of approximately 40° the model tends to be too stiff (Figure 18). The results of the detailed neck model are again slightly worse than the results of the less detailed one. However, both models fulfil the requirements of the certification test.

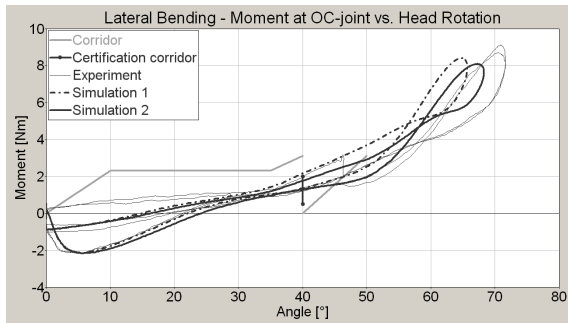


**Figure 18. Neck lateral flexion performance in pendulum test.**

The differences of the neck rubber material, validated for sled tests and for pendulum, are very little. Therefore the rubber material validated by using the neck sled tests was finally chosen. A softer neck cable, used in the pendulum simulations, also improves the neck response in the neck sled test configuration.

Both current versions of neck models were not validated to correlate also to the neck tension force  $F_z$ . First simulations showed an acceptable correlation between simulation and experiment. In a next step the material properties of the neck's steel cable and the neck rubber will be slightly modified to get a better response of  $F_z$ .

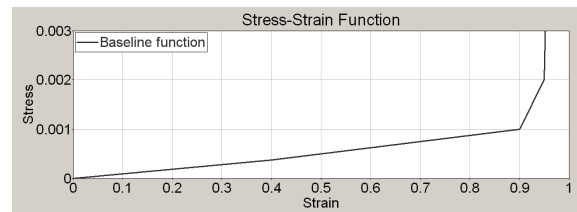
A decision, what neck model will finally be used for the dummy model has not been made yet. The final selection depends on the results of additional tests to

check the numerical robustness of the model and the head and neck response in full-dummy simulations.

### Thorax

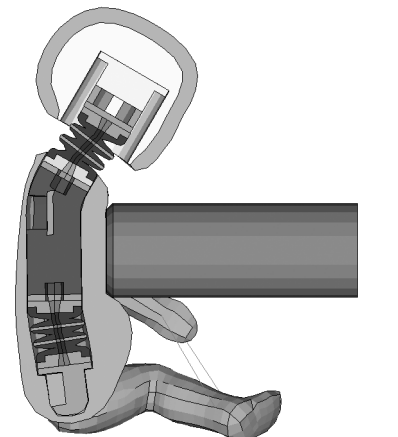
The torso foam was pre-validated by using data of drop tests. Different types of foam models were tested. Finally material MAT\_083, a Fu-Chang foam [3], was chosen. This material model is also used for the abdominal block of the LS-Dyna model of the EuroSID.

Most of the material parameters of the EuroSID foam were transferred to the Q0 model. Only the Young’s modulus  $E$ , the viscous coefficient to model damping effects (DAMP) and two stress-strain functions were varied. Both curves are based on a simple baseline stress-strain curve (Figure 19). They differ only due to scaling the magnitude of stress.



**Figure 19. Baseline stress versus strain function.**

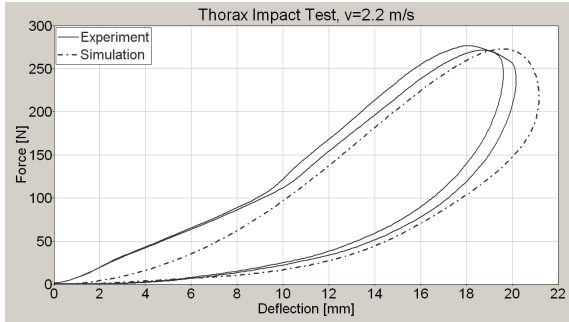
Figure 20 shows exemplarily the Q0 model in the thorax validation test at 11 ms with an impact velocity of 4.3 m/s. All parts of the model are working well together and the kinematics of head, neck and spine is realistic.



**Figure 20. Section cut of the Q0 in impactor test.**

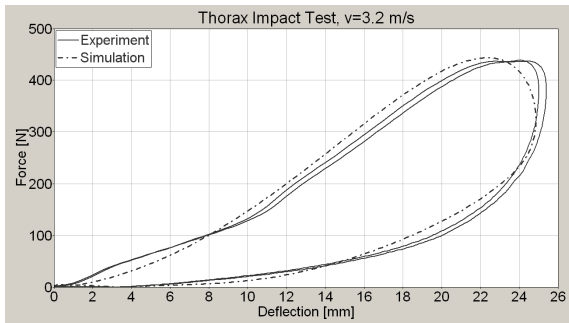
The chest deflection, calculated from chest and pendulum acceleration, is mainly influenced by the amplitude of the stress-strain functions and the material damping. Stiffer functions and higher damping reduces the chest deflection. At the same time the

impactor force, calculated from the impactor acceleration and the impactor mass, increases. However, the force is mainly affected by the amplitude of the first stress-strain curve. DAMP and E have only a very small influence on the force.



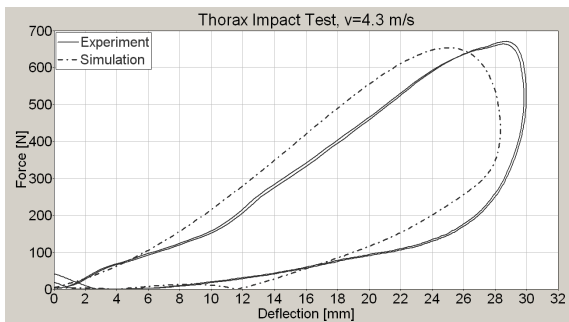
**Figure 21. Force versus deflection curve at 2.2 m/s.**

Figure 21 shows the force-deflection characteristic of the torso foam at an impact speed of 2.2 m/s. The foam is slightly too soft in this test. Especially the force during the first 10 mm of chest deflection is too low. However, the simulation is still very close to the experiment.



**Figure 22. Force versus deflection curve at 3.2 m/s.**

At an impact speed of 3.2 m/s the chest-deflection characteristic in the model is clearly closer to the experimental data (Figure 22). MAT\_083 is obviously not able to reproduce the velocity dependent effects of the torso foam in the used configuration with only two material-describing stress-strain functions.



**Figure 23. Force versus deflection curve at 4.3 m/s.**

The results of the impact test at 4.3 m/s supports this assumption (Figure 23). The foam is too stiff under these conditions. In a next step one or two functions will be added to the material model to get a better response of the foam in the three load cases.

## Extremities

Arms and legs of the Q0 dummy are made of the same material. So the same material model with the same properties was chosen for arms and legs.

The linear visco-elastic material MAT\_006 was chosen for the extremities. The maximum acceleration of the impactor is mainly influenced by GI and BETA. An increasing GI and a decreasing BETA stiffen the material and the acceleration declines.

Figure 24 shows exemplarily the results of the arm drop test with a velocity of 3.2 m/s. The simulation correlates to the experiment in this configuration as well as in the other two with different impact speeds. The maximum acceleration of the impactor with a leg mounted is too low at all three velocities tested. The deviation varies from 14% at 2.2 m/s to 5% at 4.3 m/s. It was almost impossible to validate the model for the leg impactor test. Simulations, using non-linear material models to get a better velocity-dependent response, had no drastic advantage over MAT\_006. The ratio between improvement of the response of the model and worsening of computing time was not acceptable.

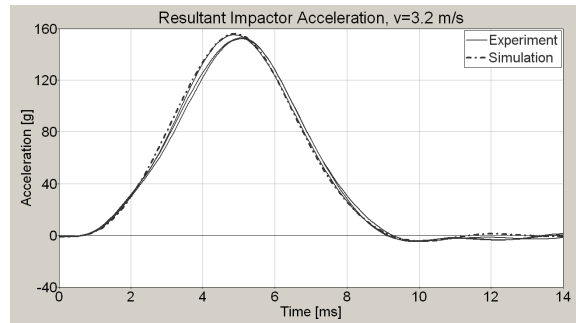


**Figure 24. Acceleration in arm drop test at 3.2 m/s.**

Figure 25 shows the resultant impactor acceleration of the leg impact test at 3.2 m/s. The increasing and the declining edge of the curve are close to the experimental data. Solely the peak value is not met.

One of the difficulties to validate the leg by using the results of drop tests could be the set-up of the tests. While the arm could easily be fixed with tape on the impactor plate and a large area of the arm had an initial contact to this plate, the fixation of the leg was difficult. Only spots at ankle, knee and thigh had an initial contact to the impactor plate. Therefore the position of

the leg was less fixed than the arm's. So the leg was able to move during the impact and its deformation. Since there were no high speed video recordings of the tests available, the kinematics of the parts could not be compared to the simulation. It was decided to validate the extremities in first priority with respect of the response of the arm and in second priority to the leg. However, the achieved results are acceptable.

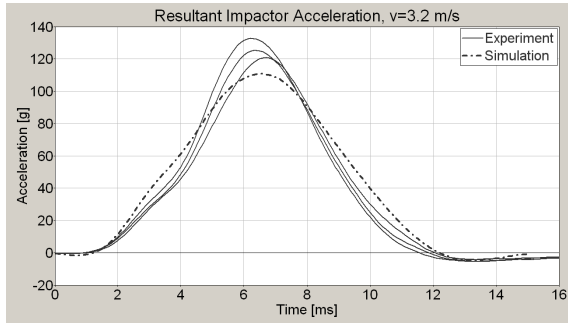


**Figure 25. Acceleration in leg drop test at 3.2 m/s.**

### Application of the Q0

Some frontal impact simulations were done with a generic Group 0+ child restraint system and a 3-point harness to tests functionality of the dummy model (Figure 26).



**Figure 26. Q0 dummy model in a infant carrier.**

It was difficult to place the dummy in the CRS because of the differences in clothing of babies and dummy. Certainly, in the current version of the model the suit is missing but it is very thin compared to diapers. A thick diaper changes the initial seating position and thus, the dummy's initial position to the harness changes as well. These differences may have an influence on the kinematics and the measured loads. In general it is easier to put a diaper on the dummy than on the dummy model.

### LIMITATIONS

Until now the dummy is made of validated sub-parts. The thorax impactor test was the only test with all assembled body segments and their interior contacts. All achieved results are promising and the remaining problems seem to be solvable. However, the Q0 dummy model was so far not tested in a validated CRS environment and numerical stability limits of the model are unknown at the moment. So it may be possible that some parts have to be modified in the next phase of the dummy development.

### FURTHER DEVELOPMENT

There is some work left to complete the development of the LS-Dyna Q0. Firstly, the response of the head will be improved by modification of the skin's FEA mesh. Secondly, the neck needs to be validated to the neck tension force  $F_z$ . Finally the response of the thorax could be improved. Therefore it is necessary to create a model of the dummy's suit.

Afterwards the dummy model will be used within CHILd for in-depth investigations of the dummy kinematics by using a CRS environment and data coming from full-scale accident reconstructions.

In parallel the model will be tested to get the limitations of the model in terms of numerical stability and the validation process.

The work on a MADYMO FEA-version of the Q0 dummy has already begun. It will be completed by end of 2005.

### CONCLUSION

The current state of the Q0 LS-Dyna model already shows a good correlation to the Q0 hardware version. All non-deformable body segments were validated by using different test set-ups or different levels of loading. So the response of the dummy segments is not only valid for a single type of loading or impact.

The resultant peak acceleration of the head is within the range of the results of two of three head drop tests. It deviates from the minimum required level by 8% in the third drop test. In a next step the FEA mesh of the head's skin layer will be modified to improve the results.

The neck response in flexion, extension and lateral bending is already close to the results of experiments using a pendulum and a sled test set-up, respectively. Furthermore a more computing time efficient version was developed. It has a lower level of detail, but the results are partly better than of the more detailed model. Until now the neck was validated in terms of

shear force, bending moment and head rotation, but it also needs to be validated in the future for a good response of the neck tension force  $F_z$ .

The extremities were validated by again using a drop test configuration. The correlation of the model's response to the experiment is acceptable as there are no requirements in the certification procedures of the dummy. There is no intention to modify the achieved level of validation.

The torso foam was validated by using results of impactor tests with the complete dummy. The overall performance of the model in terms of kinematics and response of the dummy sensors is more than acceptable. In a next step the material of the torso foam will be slightly modified to get better results at different impact velocities. Furthermore the model will be equipped with a model of the dummy's suit.

The current version of the Q0 dummy model is ready for the use within the CHILD project. It is needed for some in-depth studies of dummy kinematics and some parametric studies to support the experimental task of the project.

## ACKNOWLEDGEMENTS

The development of the Q0 dummy model is embedded in the CHILD project (G3RD-CT-2002-00791) and is funded by the European Commission. More information is available on the website <http://www.childincarsafety.com>.

The authors would like to thank TNO Automotive and FTSS Europe for supporting the work with the provision of CAD data, results of component tests and a Q0 prototype.

## REFERENCES

- [1] American Code of Federal Regulations 49, Part 572 Subpart R,
- [2] American Code of Federal Regulations 49, Part 572E
- [3] "LS-Dyna - Keyword User's Manual", Livermore Software Technology Corporation, April 2003, Version 970
- [4] Waagmeester, C. D. "Q0 Dummy User's Guide", TNO Automotive, January 23<sup>rd</sup>, 2003